TRANSITION OF STREAMWISE STREAKS IN ZERO PRESSURE GRADIENT BOUNDARY LAYERS

Luca Brandt and **Dan S. Henningson***
Department of Mechanics, KTH
S-100 44 Stockholm, Sweden
luca@mech.kth.se

INTRODUCTION

A scenario for bypass transition likely to occur in a flat plate boundary layer flow under free–stream turbulence is studied. The disturbances at the leading edge of the flat plate that show the highest potential for transient energy growth consist of streamwise aligned vortices. Due to the lift-up mechanism these optimal disturbances are transformed downstream into elongated streamwise streaks with significant spanwise modulation. The initial disturbance that yields the maximum spatial transient growth in a non-parallel flat plate boundary layer flow was determined by Andersson, Berggren and Henningson (1999) by applying the boundary layer approximations to the three-dimensional steady incompressible Navier-Stokes equations and linearizing around the Blasius base flow. If the disturbance energy of the streaks becomes sufficiently large, secondary instability can take place and provoke early breakdown and transition, overruling the theoretically predicted modal decay. A possible secondary instability is caused by inflectional profiles of the base flow velocity, a mechanism which does not rely on the presence of viscosity. Experiments with flow visualizations by for example Matsubara and Alfredsson (2001) have considered the case of transition induced by streaks formed by the passage of the fluid through the screens of the wind-tunnel settling chamber. They report on the presence of a high frequency "wiggle" of the streak with a subsequent breakdown into a turbulent spot.

In Andersson et al. (2001) Direct Numerical Simulations (DNS), using a numerical code described in Lundbladh et al. (1999), are used to follow the nonlinear saturation of the optimally growing streaks in a spatially evolving boundary layer. The complete velocity vector field from the linear results by Andersson et al. (1999) is used as input close to the leading edge and the downstream nonlinear development is monitored for different initial amplitudes of the perturbation. Inviscid secondary instability calculations using Floquet theory are performed on the obtained mean flows and it is found that the streak critical amplitude, beyond which streamwise traveling waves are excited, is about 26% of the free-stream velocity. The sinuous instability mode (either the fundamental or the subharmonic, depending on the streak amplitude) represents the most dangerous disturbance. Varicose waves are more stable, and are characterized by a critical amplitude of about 37%.

Here, also using DNS, we study the transition process resulting from the sinuous secondary instability. A velocity vector field from the simulations presented in Andersson et al. (2001) is used as inflow condition. In those simulations a spanwise antisymmetric harmonic volume force was added to the non linear streaks to trigger their sinuous secondary instability in order to check the linear stability calculations. Here the saturated streaks, $\mathbf{v_s}$, and the secondary instability mode, $\mathbf{v_d}$, obtained filtering the velocity field at the frequency ω of the forcing, are introduced as inflow condition by adding them to the Blasius solution to give the forcing vector $\mathbf{v} = \mathbf{v_0} + \mathbf{v_s} + A\mathbf{v_d}e^{i\omega t}$. An amplification factor A is used for the secondary instability to give transition within the computational box. The late stages of the process are investigated and flow structures identified. They are different from the case of transition initiated by Tollmien-Schlichting waves and their secondary instability (see Rist and Fasel 1995 as example) or by-pass transition initiated by oblique waves (Berlin et al. 1999). In these latter two scenarios Λ-vortices with strong shear layer on top, streamwise vortices deforming the mean flow and inflectional velocity profiles are observed. Berlin et al. (1999) speculated that the pattern

*Also at FOI, The Swedish Defense Research Agency, Aeronautics Division, S-17290 Stockholm, Sweden

of Λ-vortices appearing is then independent on the presence of Tollmien-Schlichting waves, but depends only on the streawise streaks and the oblique waves. These two are key elements also in the present case, but a different spatial symmetry property of the amplifying disturbance gives different flow structures. The present case shows analogies with streak instability and breakdown found in the near wall region of a turbulent boundary layer (see Schoppa and Hussain 1997 or Kawahara et al. 1998).

RESULTS

In this section we give an overview of the full transition of a streamwise streak subjected to sinuous secondary instability. Time averaged statistics and Fourier analysis of the results are presented while instantaneous flow structures are discussed in the next section. Our simulation starts at $Re_{\delta_0^*} = 875$ ($x = 0$) and if not stated differently, in the results presented the coordinates are made non dimensional using the inflow boundary layer thickness δ_0^*. The computational box is 6.86 δ_0^* wide, corresponding to one spanwise wavelength of the streak, and 10.7 δ_0^* high. A simulation with the inlet moved further downstream ($Re_{\delta^*} = 1044$) is also performed to have some fully developed turbulence within the computational box using the same number of modes. The length of the boxes is 380 δ_0^*. 1440 × 97 × 72 spectral modes are used respectively in the streamwise, wall-normal and spanwise directions.

To extract information on the frequency content of the flow, sixteen velocity field are saved during one period of the secondary instability mode. We then transform these velocity fields in time and in the spanwise direction to Fourier space and use the notation (ω, β), where ω and β are the frequency and spanwise wavenumber, each normalized with the corresponding fundamental frequency and wavenumber. The energy in some of the modes is displayed in figure 1, where the zero frequency mode represents the streak. The secondary instability mode ($\omega = 1$) is present at the beginning of the computation, while the higher harmonics are excited as the flow evolves downstream. The energy growth is exponential for a long streamwise extension and the growth rate of the first harmonic ($\omega = 2$) is twice the one of the fundamental secondary instability, and similarly for higher frequencies (not reported here), the growth rate is proportional to the harmonic order.

It is interesting to note that the energy

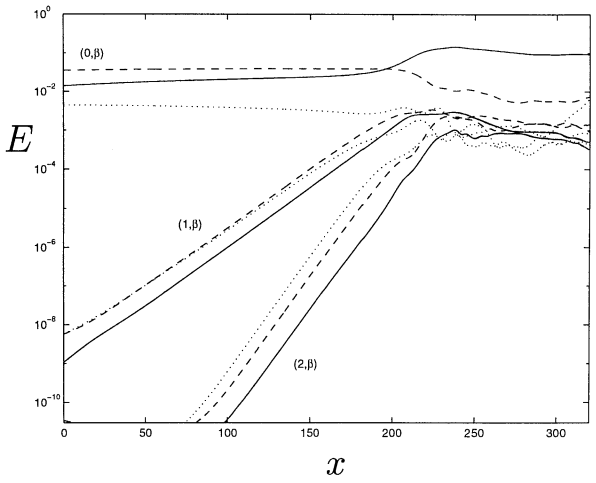

Figure 1: Energy in different Fourier modes (ω, β) versus the downstream position. Frequencies: zero (streak), one (secondary instability), two (higher harmonic). — $\beta = 0$, - - - $\beta = 1$, $\cdots$ $\beta = 2$.

content is of the same order for modes with different spanwise wavenumbers but with the same frequency. This result is different from the one obtained when the same analysis is applied to a case of transition initiated by two oblique waves (Berlin et al. 1999) or by Tollmien–Schilichting waves (Laurien and Kleiser 1989; Rist and Fasel 1995). In these cases nonlinear interactions are important to select the modes dominating the transition process, namely the streamwise independent ones, while here streaks are induced from the start and they develop to a highly nonlinear stage before they become unstable to time dependent disturbances; thus the harmonics in the spanwise direction are generated during the streak growth and are responsible for the large spanwise shear of the flow. The instability of such a flow is then characterized by modes strongly localized in the spanwise direction so that a number of wavenumbers β is needed to correctly capture them (see Andersson et al. 2001). The growth in the different harmonics starts to saturate around position $x = 200$ and soon the energy becomes of the same order for the different ω's. From this point ($x \approx 220$) the Fourier transform in time of the whole velocity fields is no longer accurate since not enough frequencies are resolved. In fact higher and higher harmonics are excited until the energy spectra fill out.

Mean velocity profiles at various locations in the transitional zone are displayed in figure 2, where the wall normal coordinate is made non dimensional with the local boundary layer thickness δ^*. The evolution from the laminar flow to a turbulent one can be seen. At position $x = 215$ a strong inflectional

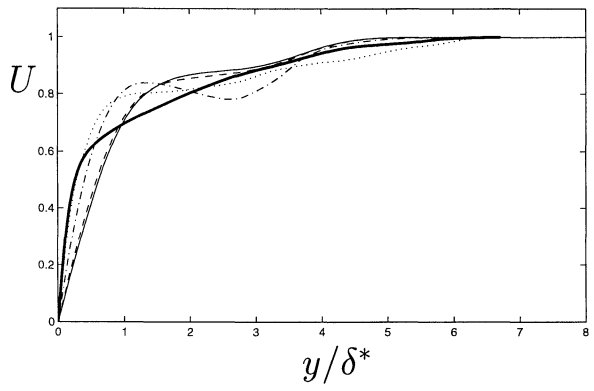

Figure 2: Average streamwise velocity in outer coordinates at different streamwise positions;$x = 126$: —— (thin line), $x = 185$: - - - , $x = 215$: - · - , $x = 268$: ··· , $x = 399$:—— (thick line).

mean profile is present exactly during the large growth of the skin friction coefficient, not reported here. In the outer part of the boundary layer one can see an over–shoot of the velocity before approaching the final value. The same behavior of the mean flow was observed by Wu et al. (1999) in their simulations of transition induced by free–stream turbulence.

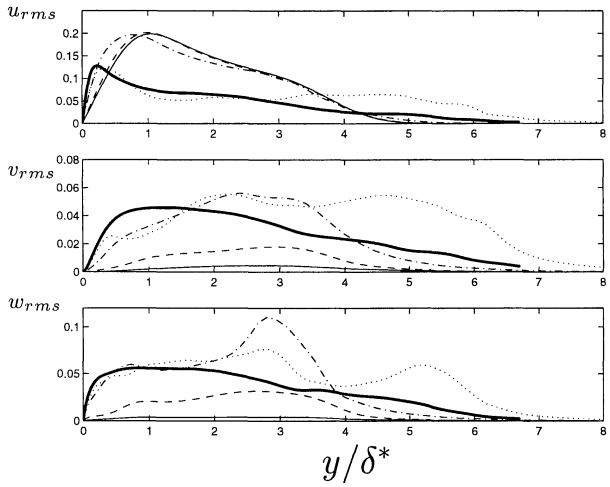

Figure 3: Time averaged Reynolds stresses in outer coordinates at different streamwise positions;$x = 126$: —— (thin line), $x = 185$: - - - , $x = 215$: - · - , $x = 268$: ··· , $x = 399$:—— (thick line).

At the early stages of transition, the averaging of the streamwise velocity provides information on the evolution of the streak during the process, since the spanwise modulation dominates in the *rms* values. These are displayed in figure 3 also for the other two velocity components. In the experiments of Matsubara and Alfredsson (2001) of transition induced by upstream–generated grid turbulence the u_{rms} value attained by the streaky structure before the breakdown is about $11 - 12\%$. In our case, instead, the streak amplitude at the beginning of transition is about 19%, but we do not have a continuous forcing by the free–stream turbulence which is able to locally nonlinearly trigger the inflectional instability of the flow. However, the same qualitative behavior of the u_{rms} is observed compared to the experiments, i.e. the peak is sharpening, moving closer to the wall and reaching values of approximatively $12 - 13\%$.

As the flow develops downstream, the *rms* values of the wall normal and spanwise velocity components increase especially in the outer part of the boundary layer, around $y \approx 3$. This corresponds to the wall normal region where the secondary instability is localized. One can also note that the spanwise velocity fluctuations are larger than the wall normal ones, and a considerable value of $w_{rms} \approx 11\%$ is attained at $x = 215$. It is also interesting to notice that at $x = 268$ the mean velocity profile, figure 2, and the u_{rms} are very close to the turbulent ones, especially close to the wall, but the v_{rms} and w_{rms} are characterized by large values in the upper part of the boundary layer. These oscillations represent periodic structures, formed in the transition region which survive downstream.

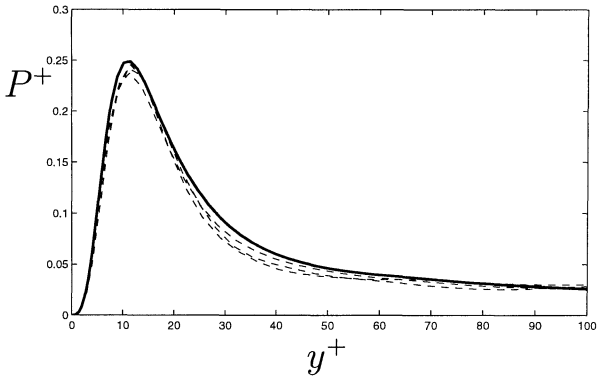

Figure 4: Time averaged non-dimensional turbulence kinetic energy production, $P^+ = -\overline{uv}^+ \frac{\partial U^+}{\partial y^+}$, near the wall. - - -: present simulations at $Re_\theta = 845$ ($x = 360$), $Re_\theta = 875$ ($x = 375$) and $Re_\theta = 910$ ($x = 400$); ——: Skote's simulations at $Re_\theta = 685$.

Profiles of the time-averaged turbulence kinetic energy production normalized with wall parameters are shown in figure 4 at the three different streamwise locations within the turbulent region and compared with the DNS data of Skote (2001). Spalart (1988) noticed that his DNS profiles of turbulent production at three different momentum thickness Reynolds numbers are self-similar. He explained it with the fact that the decrease of Reynolds stresses is compensated by the increase of mean velocity gradient for these relatively low Reynolds numbers. This seems to be true also in the present

case, since all the profiles show a maximum of $P^+ = 0.25$ at $y^+ = 12$. The agreement in the profile of the kinetic energy production let us believe that the dynamics of turbulence is active at the downstream end of our computational box. Thus the flow observed is still influenced by the deterministic inflow conditions and by the transitional process only in the upper part of the boundary layer.

INSTANTANEOUS FLOW STRUCTURES

A three-dimensional picture of the secondary instability mode is displayed in figures 5 and 6. These are obtained from the Fourier transformed velocity fields discussed in the previous section, filtering at the fundamental frequency. The mode is characterized by a streamwise wavelength $\lambda_x = 11.9$ and a frequency $\omega = 0.43$; only one wavelength λ_x is shown in the figures. Isosurface of positive and negative streamwise velocity are plotted in figure 5 to show the antisymmetry of this kind of instability. The low speed region is located around $z = 0$, where the fluctuations are stronger. The result is a spanwise oscillation of the low speed streak. The spanwise velocity, seen in figure 6, is in fact characterized by alternating positive and negative values, with a symmetric distribution of the disturbance with respect to the streak.

As observed in a number of experiments and numerical studies, see Le Cunff and Bottaro (1993) as example, the sinuous instability can be related to the spanwise inflectional points of the mean flow. Andersson et al. (2001) have shown that the secondary instability modes are concentrated around the critical layer, i.e. the layer of costant value of the mean field velocity corresponding to the phase speed of the disturbance which is $u = 0.81U_\infty$ in the present case, thus confirming the inviscid nature of the considered instability.

In figure 7 the instantaneous streamwise velocity component of the perturbation is shown in a longitudinal plane perpendicular to the wall for $z = 0$, corresponding to the center of the undisturbed low speed streak and in a plane parallel to the wall, at $y = 0.47$. The perturbation velocity field is defined as the difference between the solution velocity field and the mean value in the spanwise direction for each value of x and y. It can be clearly seen that the sinuous instability consists of harmonic antisymmetric streamwise oscillations of the low speed region.

In figure 7a) one can note that the perturbation is first seen in the outer part of the boundary layer. The disturbance moves then towards the wall until the wall-shear is considerably increased. At the end of the computational box some periodicity can still be seen in the disturbance in the outer part of the boundary layer, while close to the wall the flow is now turbulent. In figure 7b) two streaks can be seen within the computational box at the end of the transition process, with a spacing of about $130z^+$. The spanwise dimension of the

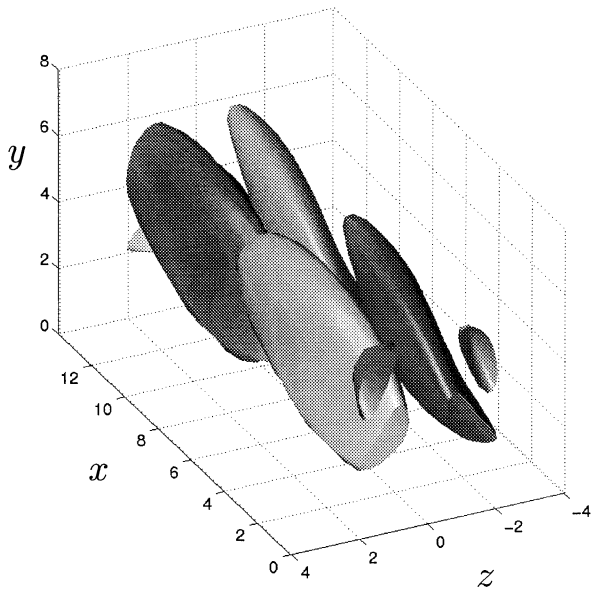

Figure 5: Isosurface of positive (dark grey) and negative (light grey) streamwise velocity component of the secondary instability eigenmode. The coordinates are made non dimensional using the local boundary layer thickness.

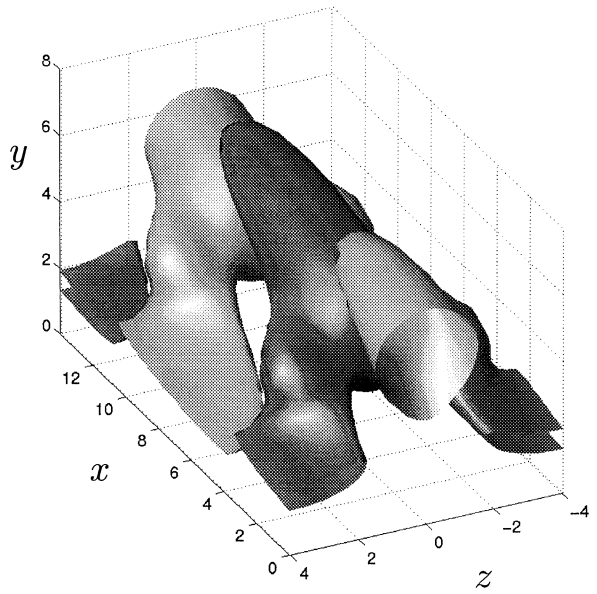

Figure 6: Isosurface of positive (dark grey) and negative (light grey) spanwise velocity component of the secondary instability eigenmode. The coordinates are made non dimensional using the local boundary layer thickness.

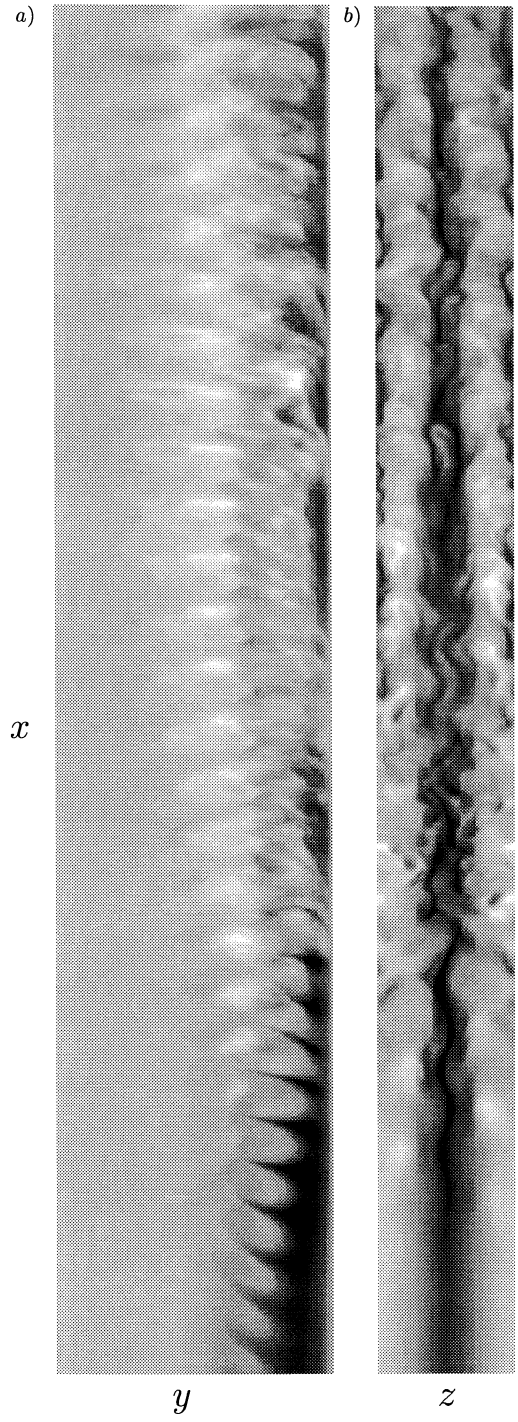

Figure 7: Visualization of streaks breakdown using streamwise velocity component of the perturbation in a wall normal x–y plane and wall parallel x–z plane. Grey scale from dark to light corresponding to negative to positive values. The flow is from bottom to top. $x-y$-plane at $z = 0$, $x-z$ plane at $y = 0.47$. $185 \leq x \leq 360$ in the streamwise direction.

box is in fact for $x > 350$ less than 275 plus units, larger than the minimal channel studied by Jiménez and Moin (1991), in which a turbulent flow could be sustained. On the other hand, the computational box is apparently too small to allow the formation of some of the large structures present in the outer region.

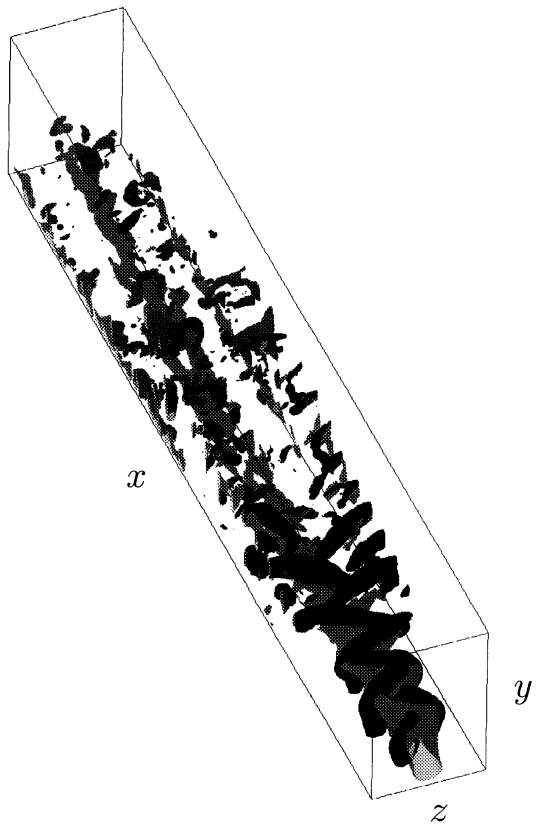

Figure 8: The flow field from the laminar to the turbulent region. The x-values correspond to the range $185 \leq x \leq 360$. The light grey structures are the low speed streaks and the darker ones are regions with low pressure. Contours level are -0.14 for the steamwise velocity fluctuations and -0.014 for the pressure for $x < 268$ and -0.0065 further downstream. The streamwise scale is one third of the cross stream ones.

The flow field from the laminar to the turbulent region is shown in figure 8. The light grey isosurface represents the low speed streaks, while the dark grey represents regions of low pressure. These corresponds to strong rotational fluid motions and are used to identify vortices. Also visualizations using negative values of the second largest eigenvalue of the Hessian of the pressure (see Jeong and Hussain 1997) are performed and no relevant differences are observed. The main structures observed during the transition process consist of elongated quasi-streamwise vortices located on the flanks of the low speed streak. Vortices of alternating sign are overlapping in the streamwise direction in a staggered pattern and they are symmetric counterparts, both inclined away from the wall and tilted in the downstream direction towards the middle of the undisturbed low speed region. The strength and extension of these vortices and the spanwise motion of the low speed streak increase downstream be-

fore the breakdown. Towards the end of the box the flow has a more turbulent nature and more complicated low-pressure structures occur. It also seems that there is no connection between the laminar and turbulent-region low speed streak, since the streak is disrupted at transition and those which appear downstream are not a continuation from upstream.

In other studied transition scenarios (Rist and Fasel 1995, Berlin et al. 1999), positive and negative streamwise vortices are also present on the side of the low speed region but they are not staggered in the streamwise direction so that the typical Λ-structures are seen. This is due to the different symmetry of the streamwise vorticity of the fundamental secondary instability; in the present case the vorticity disturbance is symmetric, while in the varicose case, observed in the simulations of oblique transition by Berlin et al. (1999), the streamwise vorticity is antisymmetric.

The vortex structures present in a turbulent boundary layer seem to be related to streak instabilities. Waleffe (1997) found that the dominating instability is sinuous and it is correlated with the spanwise inflection of the basic mean flow. Kawahara et al. (1998) and Schoppa and Hussain (1997) also used a similar approach and showed that the varicose mode is stable. The identified structures show a close resemblance to the one detected in our transitional boundary layer (Schoppa and Hussain 1997). On the other hand, Skote et al. (2001) show that the appearance of an unstable wall-normal velocity profile is a precursor to the appearance of horseshoe vortices, thus associated to varicose instability of the turbulent streaks.

References

Andersson, P., Berggren, M. and Henningson, D. S., 1999, "Optimal disturbances and bypass transition in boundary layers", *Phys. Fluids*, Vol. 11, pp. 134-150.

Andersson, P., Brandt, L., Bottaro, A. and Henningson, D. S., 2001, "On the breakdown of boundary layer streaks", *J. Fluid Mech.*, Vol. 428, pp. 29-60.

Berlin, S., Wiegel, M. and Henningson, D. S., 1999, "Numerical and experimental investigations of oblique boundary layer transition", *J. Fluid Mech.*, Vol. 393, pp. 23-57.

Jeong, J. and Hussain, F., 1997, "Coherent structures near the wall in a turbulent channel flow", *J. Fluid Mech.*, Vol. 332, pp. 185-214.

Jiménez, J. and Moin, P., 1991, "The minimal flow unit in near-wall turbulence", *J. Fluid Mech.*, Vol. 225, pp. 213-240.

Kawahara, G., Jiménez, J., Uhlmann, M. and Pinelli, A., 1998, "The instability of streaks in near-wall turbulence." Center for Turbulence Research, Annual Research Briefs 1998, pp 155-170.

Le Cunff, C. and Bottaro, A., 1993,"Linear stability of shear profiles and relation to the secondary instability of the Dean flow", *Phys. Fluids A*, Vol. 5, pp. 2161.

Laurien, E. and Kleiser, L., 1989, "Numerical simulation of boundary-layer transition and transition control", *J. Fluid Mech.*, Vol. 199, pp. 403-440.

Lundbladh, A., Berlin, S., Skote, M., Hildings, C., Choi, J., Kim, J. and Henningson, D. S., 1999, "An efficient spectral method for simulation of incompressible flow over a flat plate" TRITA-MEK Technical Report 1999:11, Royal Institute of Technology, Stockholm, Sweden.

Matsubara, M. and Alfredsson, P.H., 2001, "Disturbance growth in boundary layers subjected to free-stream turbulence", *J. Fluid Mech.*, Vol. 430, pp. 149-168.

Rist, U. and Fasel, H., 1995, "Direct numerical simulation of controlled transition in a flat-plate boundary layer", *J. Fluid Mech.*, Vol. 298, pp. 211-248.

Schoppa, W. and Hussain, F., 1997, "Genesis and dynamics of coherent structures in near-wall turbulence: a new look." In *Self-Sustaining Mechanisms of Wall Turbulence.* (ed. R. L. Panton), pp. 385-422. Computational Mechanics Publications, Southampton.

Skote, M., Haritonidis, J. H. and Heningson, D. S., 2001,"Instabilities in turbulent boundary layers", *Phys. Fluids*, submitted.

Skote, M., 2001, "Studies of turbulent boundary layer flow through direct numerical simulation", PhD thesis, Royal Institute of Technology, Stockholm, Sweden.

Spalart, P. R., 1988, "Direct siulation of a turbulent boundary layer up to $Re_\theta = 1410$.", *J. Fluid Mech.*, Vol. 197, pp. 61-98.

Waleffe, F., 1997, "On a self-sustaining process in shear flows", *Phys. Fluids*, Vol. 9, pp. 883-900.

Wu, X., Jacobs, R. G., Hunt, J. C. R. and Durbin, P. A., 1999, "Simulation of boundary layer transition induced by periodically passing wakes", *J. Fluid Mech.*, Vol. 398, pp. 109-153.